

# Photoelectron anisotropy and channel branching ratios in the detachment of solvated iodide cluster anions

Richard Mabbs, Eric Surber, and Andrei Sanov

*Department of Chemistry, University of Arizona, Tucson, Arizona 85721-0041*

(Received 16 August 2004; accepted 4 November 2004; published online 18 January 2005)

Photoelectron spectra and angular distributions in 267 nm detachment of the  $\text{I}^- \cdot \text{Ar}$ ,  $\text{I}^- \cdot \text{H}_2\text{O}$ ,  $\text{I}^- \cdot \text{CH}_3\text{I}$ , and  $\text{I}^- \cdot \text{CH}_3\text{CN}$  cluster anions are examined in comparison with bare  $\text{I}^-$  using velocity-map photoelectron imaging. In all cases, features are observed that correlate to two channels producing either  $\text{I}(^2P_{3/2})$  or  $\text{I}(^2P_{1/2})$ . In the photodetachment of  $\text{I}^-$  and  $\text{I}^- \cdot \text{Ar}$ , the branching ratios of the  $^2P_{1/2}$  and  $^2P_{3/2}$  channels are observed to be  $\approx 0.4$ , in both cases falling short of the statistical ratio of 0.5. For  $\text{I}^- \cdot \text{H}_2\text{O}$  and  $\text{I}^- \cdot \text{CH}_3\text{I}$ , the  $^2P_{1/2}$  to  $^2P_{3/2}$  branching ratios are greater by a factor of 1.6 compared to the bare iodide case. The relative enhancement of the  $^2P_{1/2}$  channel is attributed to dipole effects on the final-state continuum wave function in the presence of polar solvents. For  $\text{I}^- \cdot \text{CH}_3\text{CN}$  the  $^2P_{1/2}$  to  $^2P_{3/2}$  ratio falls again, most likely due to the proximity of the detachment threshold in the excited spin-orbit channel. The photoelectron angular distributions in the photodetachment of  $\text{I}^-$ ,  $\text{I}^- \cdot \text{Ar}$ ,  $\text{I}^- \cdot \text{H}_2\text{O}$ , and  $\text{I}^- \cdot \text{CH}_3\text{CN}$  are understood within the framework of direct detachment from  $\text{I}^-$ . Hence, the corresponding anisotropy parameters are modeled using variants of the Cooper-Zare central-potential model for atomic-anion photodetachment. In contrast,  $\text{I}^- \cdot \text{CH}_3\text{I}$  yields nearly isotropic photoelectron angular distributions in both detachment channels. The implications of this anomalous behavior are discussed with reference to alternative mechanisms, affording the solvent molecule an active role in the electron ejection process. © 2005 American Institute of Physics. [DOI: 10.1063/1.1839861]

## I. INTRODUCTION

Due to the elegant convenience of simultaneously measuring both the speed and angular distributions, the imaging technique<sup>1</sup> has become a widely accepted tool in the studies of neutral and charged species in gas-phase experiments.<sup>2,3</sup> The imaging approach to negative-ion photoelectron spectroscopy<sup>4</sup> allows distinct advantages. First, photoelectron spectra can be measured with uniform sensitivity for all electron kinetic energies (eKE), up to the maximum-eKE limit of the detection range. This feature of imaging proved to be extremely beneficial in probing near-threshold and indirect detachment processes that yield low-eKE electrons.<sup>5-7</sup> Second, the energy-resolved photoelectron angular distributions (PAD) are also determined in a straightforward manner, providing direct and often highly visual insights into the electronic structure of the parent anions.<sup>8-10</sup> In recent years, these facets of imaging have been applied to atomic, molecular, and cluster anions, yielding a wealth of information about the species from which the detachment takes place.<sup>5,6,8-18</sup> The technique also shows promise as a tool to study the evolution of the electronic structure as a chemical reaction unfolds, serving as a powerful extension of femtosecond photoelectron spectroscopy.<sup>19-22</sup>

In using photoelectron images to elucidate the electronic structure of parent anions, the effect of surrounding molecules needs to be understood. Intermolecular interactions are the focus of the studies of clusters<sup>23-25</sup> and collision processes. They also play an important role in time-resolved dissociation experiments, since the fragments necessarily start out in close proximity. These considerations motivate

our continuing studies of the effect of solvent interactions on the electronic structure of anions, with a particular emphasis on the PADs arising from the photodetachment processes.

We have recently carried out a series of photodetachment imaging experiments on cluster anions involving molecular core-anion and solvent species.<sup>8,10,14,17,18</sup> These studies shed light on the electrostatic and covalent interactions implicated in homogenous and heterogeneous solvation of molecular anions. In the present work, we turn to solvent-induced effects in the photodetachment of an atomic anion. The reduced number of degrees of freedom and the availability of tested theoretical models pertaining to atomic-anion photodetachment, coupled with the advantages afforded by imaging, allow for more detailed understanding of solvation effects on the photodetachment dynamics.

The core anion chosen in this study is  $\text{I}^-$ . Its spectroscopy is well characterized,<sup>26-28</sup> but the channel branching ratios in the photodetachment experiments warrant additional discussion.<sup>29</sup> Four solvent species ( $\text{Ar}$ ,  $\text{H}_2\text{O}$ ,  $\text{CH}_3\text{I}$ , and  $\text{CH}_3\text{CN}$ ) are chosen to examine the effects of solvation on the electronic structure and detachment dynamics. The choice of the solvation partners is dictated by the different interactions implicated in the corresponding cluster anions. The  $\text{I}^- \cdot \text{Ar}$  anion is a relatively weakly bound cluster, in which the dominant interaction is due to the polarizability of the closed-shell, spherically symmetric  $\text{Ar}$  atom. The molecular solvents are bound to the anion by stronger electrostatic interactions involving significant dipole moments, which can potentially affect not only the energetics but also the dynamics of the detachment. While this is the case for all

three molecular solvents studied, only  $\text{CH}_3\text{CN}$  is capable of forming a dipole-bound anion in isolation.<sup>30,31</sup> Methyl iodide is also of special interest, because the structure of  $\text{I}^- \cdot \text{CH}_3\text{I}$  cluster anion is representative of the entrance channel of the  $\text{S}_{\text{N}}2$  reaction  $\text{I}^- + \text{CH}_3\text{I} \rightarrow \text{ICH}_3 + \text{I}^-$ .<sup>32</sup>

The five anions in this work had been extensively studied through photoelectron and ZEKE spectroscopies<sup>30,32–43</sup> and thus the cluster structures are fairly well known. The spectra all appear to reflect the detachment from  $\text{I}^-$ , with the transition energies reflecting the solvent-induced stabilization of the bound orbitals of the anion relative to the lowest unoccupied orbital of the neutral. However, in the previous studies of  $\text{I}^- \cdot \text{Ar}$ ,  $\text{I}^- \cdot \text{H}_2\text{O}$ ,  $\text{I}^- \cdot \text{CH}_3\text{I}$ , and  $\text{I}^- \cdot \text{CH}_3\text{CN}$ , little attention was paid to the solvent-induced variations in the PADs or relative photodetachment cross sections. In the current work, advantage is taken of the photoelectron imaging technique to redress this omission, yielding in some cases surprising results.

## II. EXPERIMENTAL APPARATUS

The experimental apparatus is described in detail elsewhere.<sup>9</sup> In brief, it employs the ion generation and mass analysis techniques of Lineberger and co-workers,<sup>44,45</sup> combined with a velocity mapped,<sup>46</sup> imaging<sup>1</sup> scheme for detection of the photoelectrons.

The anions are formed in an electron impact ionized pulsed supersonic expansion of a precursor gas mixture, which includes undried carrier gas (Ar) and the desired solvent vapor, seeded with the ambient pressure of  $\text{I}_2$ . The resulting gas, at a total stagnation pressure of 40 psi (gauge), is expanded through a pulsed 70 Hz nozzle (General Valve Series 9) into a region with a base pressure of  $10^{-6}$  Torr, rising to  $2 \times 10^{-5}$  Torr when the valve is operated. For the preparation of  $\text{I}^- \cdot \text{CH}_3\text{I}$ , a 5% concentration of methyl iodide is used. For  $\text{I}^- \cdot \text{CH}_3\text{CN}$ , the ambient vapor pressure of acetonitrile is mixed with that of iodine prior to expansion. In the experiments on  $\text{I}^- \cdot \text{H}_2\text{O}$ , residual vapor within the gas delivery lines serves as a source of  $\text{H}_2\text{O}$ .

The supersonic expansion is crossed with a 1 keV electron beam and the resulting anions are pulse extracted into a Wiley-McLaren time-of-flight mass spectrometer.<sup>47</sup> Toward the end of the flight tube, the ions enter the detection region with a typical base pressure of  $3 \times 10^{-9}$ – $5 \times 10^{-9}$  Torr, where mass spectra are recorded using a dual microchannel plate (MCP) detector (Burle, Inc.). Prior to impacting the detector, the ion beam is crossed with the frequency tripled output from an amplified Ti:Sapphire laser system (Spectra Physics, Inc., 1 mJ, 100 fs pulses at 800 nm). The 267 nm light is generated by mixing the fundamental and the second harmonic in the super tripler harmonics generator (Super Optonics, Inc.), giving 20  $\mu\text{J}/\text{pulse}$  with a 4.4 nm bandwidth. The linearly polarized beam is mildly focused using a 1 m focal length lens positioned  $\approx 0.5$  m before the crossing of the laser and ion beams.

Photoelectrons are detected in the direction perpendicular to the plane containing the ion and laser beams. A 40 mm diameter MCP detector with a P47 phosphor screen (Burle, Inc.) is mounted at the end of an internally  $\mu$ -metal shielded

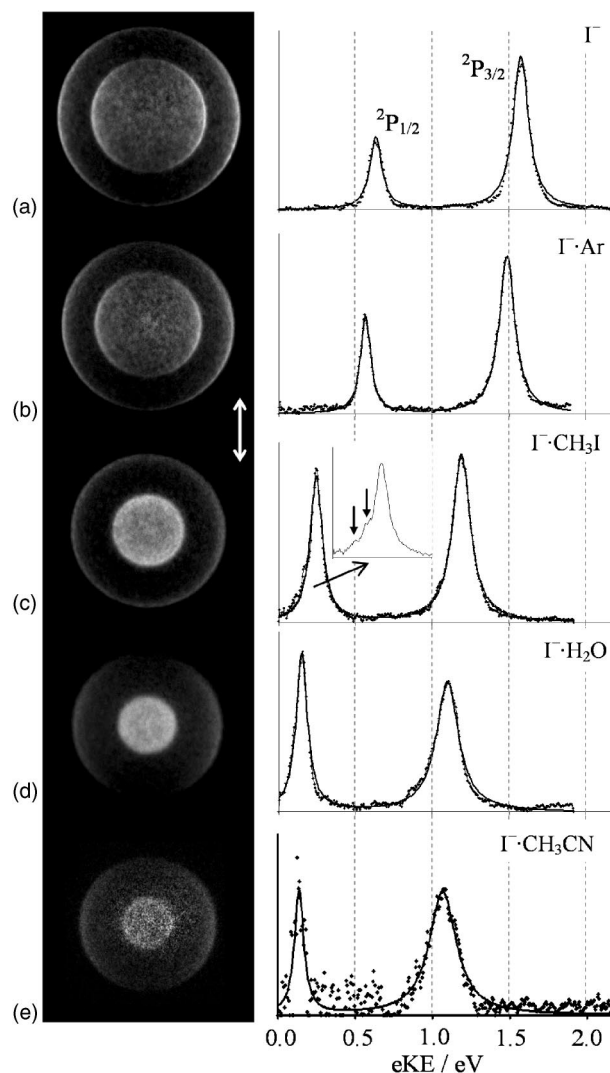


FIG. 1. Photoelectron images and the corresponding spectra obtained in 267 nm detachment of (a)  $\text{I}^-$ , (b)  $\text{I}^- \cdot \text{Ar}$ , (c)  $\text{I}^- \cdot \text{CH}_3\text{I}$ , (d)  $\text{I}^- \cdot \text{H}_2\text{O}$ , and (e)  $\text{I}^- \cdot \text{CH}_3\text{CN}$ . The images and spectra are displayed on arbitrary intensity scales; however, the electron focusing conditions are the same in each image allowing a direct visual comparison of the eKEs. The detachment laser is polarized vertically in the image plane, as indicated by the double arrow. Smooth solid lines through the data represent Lorentzian fits to the observed spectral peaks. The inset in (c) shows an expanded portion of the  $\text{I}^- \cdot \text{CH}_3\text{I}$  spectrum with arrows indicating the partially resolved vibrational structure in the (asymptotic)  $^2P_{1/2}$  channel.

electron flight tube. The direction of the laser polarization is maintained parallel to the imaging detector plane, as required for data analysis based on the inverse Abel transformation techniques.<sup>2,48</sup> Images are recorded from the phosphor screen using a charge-coupled device (CCD) camera (CoolSnap, Roper Scientific, Inc.) and are typically averaged for  $(1-3) \times 10^4$  experimental cycles. To discriminate against experimental noise, the potential difference across the two imaging MCPs, maintained at 1.0–1.2 kV total, is pulsed up to the normal operational level of 1.8 kV for a 200 ns window timed to coincide with the arrival of the photoelectrons.

## III. RESULTS AND ANALYSIS

Figure 1 shows the raw photoelectron images obtained in 267 nm detachment of  $\text{I}^-$  and  $\text{I}^- \cdot M$  ( $M = \text{Ar}, \text{CH}_3\text{I}$ ,

TABLE I. Spectral and angular distribution parameters and channel branching ratios determined from the photoelectron images in Fig. 1.

Anionic species	Peak eKE (eV)		Spectral shift (eV)		$\beta$		Branching ratio ${}^2P_{1/2} : {}^2P_{3/2}$
	${}^2P_{3/2}$	${}^2P_{1/2}$	${}^2P_{3/2}$	${}^2P_{1/2}$	${}^2P_{3/2}$	${}^2P_{1/2}$	
$I^-$	1.57	0.63			-0.67	-0.73	0.38 ( $\pm 0.01$ )
$I^- \cdot Ar$	1.53	0.58	0.04	0.05	-0.70	-0.69	0.40 ( $\pm 0.01$ )
$I^- \cdot CH_3I$	1.21	0.26	0.36	0.37	-0.26	0.02	0.60 ( $\pm 0.01$ )
$I^- \cdot H_2O$	1.11	0.16	0.46	0.47	-0.77	-0.13	0.63 ( $\pm 0.01$ )
$I^- \cdot CH_3CN$	1.10	0.14	0.47	0.49	-0.70	-0.10	0.35 ( $\pm 0.03$ )

$H_2O, CH_3CN$ ). Also shown are the corresponding photoelectron energy spectra. Each image displays two concentric circular bands corresponding to the  $I^-({}^1S_0) \rightarrow I({}^2P_{3/2}) + e^-$  and  $I^-({}^1S_0) \rightarrow I({}^2P_{1/2}) + e^-$  detachment channels in the core iodide anion, hereafter referred to as the  ${}^2P_{3/2}$  and  ${}^2P_{1/2}$  transitions, respectively. The outer bands, corresponding to faster photoelectrons, are ascribed to the energetically lower,  ${}^2P_{3/2}$  detachment channel, while the inner bands correspond to the excited  ${}^2P_{1/2}$  spin-orbit state of the neutral I atom formed in the photodetachment.

All images in Fig. 1 were recorded under the same electron imaging lens<sup>46</sup> conditions and are presented on the same velocity scale. Thus, the radii of the bands, which vary with  $M$ , reflect the solvent-dependent energetics of the electron detachment. In addition, the following two effects are apparent upon inspection of the images. First, a significant enhancement of the excited spin-orbit channel is observed in the detachment of  $I^- \cdot H_2O$  and  $I^- \cdot CH_3I$ , compared to  $I^-$ ,  $I^- \cdot Ar$ , and  $I^- \cdot CH_3CN$ . The increased relative intensities of the inner rings in Figs. 1(c) and 1(d), compared to Figs. 1(a), 1(b), and 1(e), are easily seen by eye. Second, there is a striking loss of anisotropy in the angular distribution of *both* transitions in  $I^- \cdot CH_3I$ , as seen in Fig. 1(c). The (nearly) isotropic PAD contrasts this cluster anion with all other systems studied in this work.

The images in Fig. 1 represent the projections on the detector plane of the probability density distributions (i.e.,  $|\psi|^2$ ) of the final state of the photodetached electron in the three-dimensional linear-momentum (velocity) space, averaged over random orientations of the parent anions in the laboratory frame. To determine the corresponding energy and angular distributions, the original three-dimensional distributions must be reconstructed. This task is accomplished by the inverse Abel transformation,<sup>2</sup> which makes use of the cylindrical symmetry imposed on the photoelectrons by the linear polarization of light used in photodetachment. In this work, the analysis is carried out using the Reisler group's basis set expansion program (BASEX),<sup>48</sup> which yields both the energy spectra and PADs corresponding to the experimental images.

The photoelectron spectrum of  $I^-$  in Fig. 1(a) exhibits two transitions corresponding to the two spin-orbit channels, separated by 0.94 eV. The widths of the peaks reflect the convolution of the laser bandwidth with other experimental broadening factors. The stabilizing effect of the solvent is clearly seen in the cluster-anion spectra, where the transi-

tions are shifted to lower eKE compared to  $I^-$ . The data in Figs. 1(b)–1(e) are presented in order of increasing solvation energy. The spectra were analyzed through Lorentzian line fitting and thus determined positions of the transition maxima, along with the magnitudes of the solvent-induced spectral shifts, are summarized in Table I.

Of the advantages of imaging discussed in the Introduction, particularly important for this work is the uniform detection sensitivity for all photoelectrons up to the maximum-eKE limit. This experimental feature provides for an accurate determination of the channel branching ratios, which can be obtained from the integrated spectral peak intensities deduced from the Lorentzian fits. The  ${}^2P_{1/2}$  to  ${}^2P_{3/2}$  channel branching ratios obtained in this work are summarized in Table I. Consistent with the qualitative features of the images in Fig. 1, the branching ratios show a dramatic increase for  $I^- \cdot CH_3I$  and  $I^- \cdot H_2O$  compared to bare  $I^-$  and  $I^- \cdot Ar$ . However, the ratio decreases again for detachment from  $I^- \cdot CH_3CN$ .

In the  $I^- \cdot CH_3I$  case, additional structure, discussed previously by Johnson and co-workers,<sup>32,49</sup> can be discerned in the photoelectron spectrum in Fig. 1(c). Although too weak to have a significant effect on the Lorentzian peak fitting procedure, this structure is superimposed on the lower-eKE wings of both spin-orbit channels. While hardly seen in the  ${}^2P_{3/2}$  channel, it is partially resolved in the  ${}^2P_{1/2}$  band, as shown in the inset in Fig. 1(c). Its emergence in the excited spin-orbit channel is due to the improved absolute energy resolution for slower photoelectrons. The approximate spacing of  $560 \text{ cm}^{-1}$  between the features on the  ${}^2P_{1/2}$  band wing is consistent with excitation of the C–I stretch in neutral  $CH_3I$ .<sup>32,49</sup>

The PADs resulting from one-photon detachment using linearly polarized light can be, in general, characterized by the anisotropy parameter  $\beta$ ,<sup>50–52</sup> determined by fitting the function

$$I(\theta) = (\sigma/4\pi)[1 + \beta P_2(\cos \theta)] \quad (1)$$

to the angular distributions derived from the images. In Eq. (1),  $\sigma$  is the total detachment cross section, used here as an arbitrary fitting parameter,  $\theta$  is the angle between the laser polarization axis, and the photoelectron velocity vector, and  $P_2(\cos \theta)$  is the second-order Legendre polynomial. The  $\beta$  values obtained from the images in Fig. 1 are summarized in Table I.

#### IV. DISCUSSION

In many cluster anions, the excess electron is largely localized on a well-defined core moiety. In the cluster anions studied in this work, this moiety is the iodine atom, its electron affinity being much greater than that of any of the solvating species used.<sup>53</sup> When considering the detachment processes in these clusters, a logical starting point is the photodetachment from bare  $I^-$ . By itself,  $I^-$  is a closed shell species, for which the lowest detachment transition, under the one-electron approximation, involves removal of an electron from a  $5p$  atomic orbital. Spin-orbit interaction in the residual open-shell atom gives rise to two distinct final states, the lower  $^2P_{3/2}$  state and the upper  $^2P_{1/2}$  state, separated by 0.94 eV.<sup>26</sup> All photoelectron images in this work bear signatures of  $I^-$  photodetachment with narrow spectral features.

We will discuss two types of solvent effects. The first concerns the  $^2P_{1/2}:^2P_{3/2}$  transition branching ratio, which varies significantly throughout the series of the cluster anions studied. The second concerns the photoelectron anisotropy, particularly the anomalously nearly isotropic nature of  $I^- \cdot CH_3I$  photodetachment. The starting point for these discussions is the detachment of  $I^-$ , which is used as a reference system for interpreting the results for the solvated species.

##### A. Branching ratios

In  $I^-$  photodetachment, the statistical  $^2P_{1/2}:^2P_{3/2}$  channel branching ratio is 0.5, as determined by the  $(2J+1)$ -fold degeneracy of the corresponding  $^2P_J$  neutral states. The branching ratio of 0.38 observed in the photodetachment of bare  $I^-$  deviates from this expectation, indicating that the final-state populations are determined not only by the channel statistics, but also by the relative cross sections, which are in turn affected by the dynamics of photodetachment.

In  $I^-$ , the initial state of the electron is characterized by the orbital angular momentum quantum number  $\ell=1$ . Under the electric-dipole selection rule,  $s$  and  $d$  partial waves are formed in the one-photon process. Unlike photoionization of a neutral atom, in negative-ion photodetachment the departing electron interacts with a neutral residue, with no Coulomb attraction. The shorter-range higher-order interactions, for which the magnitude of the long-range potential decays faster than  $1/r^2$ , are not sufficient to suppress the centrifugal barrier for waves with  $\ell>0$ . Therefore, the corresponding partial cross-sections scale differently with eKE, generally conforming to the Wigner law near the detachment threshold.<sup>54</sup>

The photon energy employed in the current work is some way from threshold and the purely Wigner region,<sup>55</sup> however, the overall qualitative trend in channel cross sections in this energy regime is to increase with eKE. Owing to this trend, one expects larger cross sections per  $M_J$ -channel in the detachment leading to the  $^2P_{3/2}$  neutral state, compared to  $^2P_{1/2}$ . ( $M_J$  denotes the quantum number for the projection of the total electronic angular momentum). The greater cross sections for  $I^- \rightarrow I(^2P_{3/2}) + e^-$  detachment, compared to  $I^- \rightarrow I(^2P_{1/2}) + e^-$ , result in a smaller than statistical  $^2P_{1/2}:^2P_{3/2}$  branching ratio, as observed in the experiment.

This analysis is further supported by available quantita-

tive treatments of  $I^-$  photodetachment. Several one-electron models have been used to predict detachment cross sections.<sup>28,56–63</sup> These semiempirical treatments have been applied with some success to detachment leading to a ground-state neutral atom. However, ignoring many-body interactions and the effect of the remaining neutral core on the detachment process, inherent in the one-electron models, limits their success in applications to highly polarizable atoms, as well as atoms with large electron affinities and detachment channels leading to excited neutral states.

More accurate treatments taking into account many-body effects are outlined in a review by Ivanov.<sup>64</sup> Methods based on the relativistic random phase approximation,<sup>65–67</sup> have been applied to the study of halide-anion detachment cross sections. For detachment from the  $5p$  orbital, the branching ratio is predicted to favor the  $^2P_{3/2}$  neutral state with a greater than statistical weight for photon energies up to  $\sim 9$  eV. The experimentally observed nonstatistical  $^2P_{1/2}:^2P_{3/2}$  branching ratio of 0.38 is in good agreement with the prediction by Kutzner *et al.*<sup>67</sup> Thus, although 267 nm is sufficiently far from both detachment thresholds for cross sections to deviate from the Wigner law, the partial cross sections are still increasing with photoelectron energy in this energy range. Hence, the energy difference between the two neutral states causes the observed deviation from statistical behavior.

The  $^2P_{1/2}:^2P_{3/2}$  branching ratio shows significant changes caused by interaction with different solvation partners (see Table I). The  $I^- \cdot Ar$  data yield a branching ratio similar to that for  $I^-$ , suggesting that Ar has little effect on the cross section for either detachment channel. This is not the case for  $I^- \cdot CH_3I$  and  $I^- \cdot H_2O$ , for which the branching ratios indicate a relative enhancement of the  $^2P_{1/2}$  channel compared to bare  $I^-$ . In interpreting these data, it is helpful to examine the effects of solvation on photodetachment cross sections observed elsewhere.

Johnson and co-workers measured the total detachment cross section as a function of wavelength for the series of hydrated iodide clusters  $I^-(H_2O)_n$ ,  $n=0-6$ .<sup>34</sup> Their experiments showed that hydration changes the detachment trends. For bare  $I^-$ , the total cross section rises gradually with energy above the  $^2P_{3/2}$  threshold and shows another sharp increase at the  $^2P_{1/2}$  channel opening. In the presence of water molecules, it exhibits a well-defined maximum above the  $^2P_{3/2}$  threshold followed by a decrease all the way to the  $^2P_{1/2}$  channel opening, which marks another sharp rise and a subsequent decrease. Another striking example of near-threshold enhancement of the detachment cross section is found in the Johnson's group work on  $I^- \cdot CH_3CN$ ,<sup>29</sup> where the cross section is dominated by a sharp near-threshold peak attributed to a dipole-bound state.

The existence of cross-section maxima indicates competition of two different trends. The first is the overall increase in detachment cross sections with increasing energy, as discussed above for the bare  $I^-$  case. The second, hydration-induced mechanism works in the opposite direction, increasing the cross sections in the near-threshold regions of small eKE. Johnson's explanation for the enhanced near-threshold cross sections invokes the long-range attractive potential due to the polar water molecules, which partially localizes the

final-state continuum wave function in the vicinity of the core.<sup>34</sup> As the energy increases, the cross section for a given channel drops, as the continuum wave function becomes more delocalized, reducing its overlap with the initial bound state.

With regard to the present measurements, we are nearer threshold in the  ${}^2P_{1/2}$  channel, and hence its cross section is relatively enhanced in a similar way in the presence of polar solvents. Thus, the localization of the continuum wave function near the core, suggested by Johnson and co-workers,<sup>34</sup> can explain the increased yield of the upper spin-orbit channel in  $\text{I}^- \cdot \text{H}_2\text{O}$  and  $\text{I}^- \cdot \text{CH}_3\text{I}$  photodetachment observed in this work.

However, the branching ratio for  $\text{I}^- \cdot \text{CH}_3\text{CN}$ , when compared to  $\text{I}^-$ ,  $\text{I}^- \cdot \text{H}_2\text{O}$  and  $\text{I}^- \cdot \text{CH}_3\text{I}$  (see Table I), does not appear to follow this trend. Several tentative explanations may be advanced for this behavior. It is unlikely that the difference between the  $\text{I}^- \cdot \text{CH}_3\text{CN}$  branching ratio and those exhibited by  $\text{I}^- \cdot \text{H}_2\text{O}$  and  $\text{I}^- \cdot \text{CH}_3\text{I}$  reflects competition between direct photodetachment and autodetachment. The evidence against this is seen in the highly anisotropic nature of the PADs arising from both  $\text{I}^- \cdot \text{H}_2\text{O}$  and  $\text{I}^- \cdot \text{CH}_3\text{CN}$ , which is characteristic of a direct process. One must also keep in mind that unlike the work of Johnson and co-workers,<sup>34</sup> we measure the branching ratio at a single energy only. The  ${}^2P_{1/2}$  channel threshold in  $\text{I}^- \cdot \text{CH}_3\text{CN}$  is quite close to the 267 nm photon energy, giving  $e\text{KE}=0.14$  eV. In this regime, the continuum wave function is dominated by  $s$ -wave detachment, whose cross section diminishes rapidly with decreasing  $e\text{KE}$  (as  $\propto e\text{KE}^{1/2}$  in a pure Wigner case). Being closer to the detachment threshold than any other system studied, the cross section for this channel may be correspondingly reduced by near-threshold effects. It must be pointed out, however, the difference between the electron kinetic energies in the  ${}^2P_{1/2}$  channels for  $\text{I}^- \cdot \text{H}_2\text{O}$  and  $\text{I}^- \cdot \text{CH}_3\text{CN}$  detachment is small.

The second, less likely possibility arises from the  $\text{CH}_3\text{CN}$  dipole moment that is sufficient to support a dipole-bound anion state. This state could conceivably act as a sink for the lowest- $e\text{KE}$  electrons. Dipole-bound anions have been prepared by Johnson and co-workers dissociating  $\text{I}^- \cdot \text{CH}_3\text{CN}$  at 3.496 eV, i.e., just below the vertical detachment energy.<sup>31,42</sup> However, the energy supplied in the present case is 4.6 eV, exceeding even the upper spin-orbit channel threshold by 140 meV. Varying the detachment energy may shed light on this issue. An important caveat is that if the detachment energy is increased by more than a few hundreds of meV, the  $e\text{KE}$  of the  ${}^2P_{3/2}$  channel moves into the region where dissociative electron attachment to  $\text{CH}_3\text{CN}$  may occur, yielding  $\text{CH}_3 + \text{CN}^-$ .<sup>68</sup> The opening of this additional channel will have the effect of reducing the observed  ${}^2P_{3/2}$  photodetachment cross section.

## B. Photoelectron angular distributions

Photoelectron anisotropy is known to be, in general,  $e\text{KE}$  dependent. Thus, it is no surprise that the  $\beta$  values summarized in Table I vary from image to image and, in most cases, between the transitions in a given image. Since the photodetached electron initially resides mainly on the iodine atom,

we will again begin with a discussion of its detachment as an atomic process and then examine the effects of the solvent.

In the atomic picture, the observed PAD arises from interference between the  $s$  and  $d$  partial waves formed in the detachment from a  $5p$  orbital. Cooper and Zare developed a model for photoelectron angular distributions, in which the detached electron moves in the central potential due to the atomic residue.<sup>51,52</sup> The parameters in this model are the initial orbital angular momentum quantum number  $\ell$ , the phase angles and dipole radial matrix elements  $R_{\ell'}$  corresponding to the emitted waves (described by  $\ell'=\ell\pm 1$ ). Hanstorp *et al.*<sup>69</sup> simplified this formalism by further assuming that the wavelength of the free electron is large compared to the size of the initial state and that there is no interaction between the departing electron and the neutral-atom residue. Under these assumptions, the ratio of the final-state radial matrix elements varies linearly with  $e\text{KE}$ :  $R_{\ell+1}/R_{\ell-1}=AE$ , where  $E \equiv e\text{KE}$  and  $A$  is the proportionality coefficient. This simplification allows the calculation of  $\beta$  according to the following equation:

$$\beta = \frac{\ell(\ell-1) + (\ell+1)(\ell+2)A^2E^2 - 6\ell(\ell+1)AE \cos \phi}{(2\ell+1)[\ell + (\ell+1)A^2E^2]}, \quad (2)$$

where  $\phi$  is the relative phase of the  $\ell'=\ell\pm 1$  partial waves. Hanstorp *et al.* applied this model to detachment from a  $p$  orbital in the  $\text{O}^-$  case,<sup>69</sup> where, similar to  $\text{I}^-$ ,  $AE$  is also the ratio of the  $d$  to  $s$  radial matrix elements.

The application of this model to the present data is shown in Fig. 2(a). Different symbols (with the exception of the crosses) correspond to the experimental  $\beta$  values obtained for bare  $\text{I}^-$  at various wavelengths<sup>17,22</sup> and the cluster anions studied in this work. The solid line represents Eq. (2) for  $\ell=1$ , optimized for agreement with the experimental data for  $\text{I}^-$  by varying  $A$  and  $\cos \phi$  with a nonlinear fitting procedure using the Levenberg-Marquardt method.<sup>70</sup> The parameters used are  $A=0.4932 \text{ eV}^{-1}$  and  $\cos \phi=0.8617$ . The 95% confidence and prediction limits are also shown by the dashed and dotted lines, respectively. These limits also encompass the experimental points for  $\text{I}^-$  obtained by the groups of Lineberger<sup>71</sup> and Neumark<sup>21</sup> (open squares and triangle, respectively), giving further confidence in the present results. Comparing the model predictions to the cluster-anion data, we conclude that the  $\text{I}^- \cdot M$  PADs are described well in terms of direct atomic-anion photodetachment, with the notable exception of  $\text{I}^- \cdot \text{CH}_3\text{I}$ .

In the above analysis, it was assumed that the solvent acts as a mere spectator in the process of photodetachment of atomic iodide. However, for cluster anions it may be unrealistic to assume that the neutral residue does not interact with the departing electron, especially in the case of polar solvents. The dipole moment of the neutral  $\text{I} \cdot \text{Ar}$  complex is indeed small ( $\sim 0.01$  D, estimated by an HF/3-21G calculation using GAUSSIAN98 (Ref. 72) at the experimentally determined cluster-anion geometry<sup>33</sup>). However,  $\text{I} \cdot \text{H}_2\text{O}$ ,  $\text{I} \cdot \text{CH}_3\text{I}$  and  $\text{I} \cdot \text{CH}_3\text{CN}$  are predicted to have appreciable dipole moments. For example, HF/3-21G calculations at the corresponding anion equilibrium geometries<sup>36,73</sup> give  $\mu=2.03$  D

for  $\text{I}\cdot\text{CH}_3\text{I}$ , 2.38 D for  $\text{I}\cdot\text{CH}_3\text{CN}$ , and 2.77 D for  $\text{I}\cdot\text{H}_2\text{O}$ . Hence one can expect considerable electron-dipole interactions in these systems.

The effect of these interactions on the free-electron wave cross sections can be modeled following the work of O'Malley.<sup>74</sup> In the limit of a small dipole moment of the neutral residue in near-threshold photodetachment, the cross section of a partial wave characterized by an angular momentum quantum number  $\ell'$  scales as

$$\sigma_{\ell'} \approx C_{\ell'} A_{\ell'} = C_{\ell'} k^{2\nu}, \quad (3)$$

where  $\nu = [(\ell' + 1/2)^2 - \mu]^2$ ,  $k$  is the linear momentum of the free electron and  $\mu$  is the dipole moment of the neutral

residue (in atomic units). For large  $\mu$ , the partial-wave cross section is given by<sup>74</sup>

$$\sigma_{\ell'} \approx C_{\ell'} A_{\ell'} = C_{\ell'} \{ \sinh^2(\pi\nu'/2) + \cos^2[(\nu' \ln k) + \delta] \}^{-1}, \quad (4)$$

where  $\nu' = [\mu - (\ell' + 1/2)^2]^{1/2}$  and  $\delta$  is a phase factor. The transition between the small and large dipole-moment regimes occurs at  $\mu = (\ell' + 1/2)^2$ .

The ratio of  $\sigma_{\ell+1}$  and  $\sigma_{\ell-1}$  calculated using either Eq. (3) or Eq. (4) can be used to determine the ratio of the dipole matrix elements in Eq. (2). Assuming that only the radial part varies with eKE, we obtain  $R_{\ell+1}/R_{\ell-1} = (\sigma_{\ell+1}/\sigma_{\ell-1})^{1/2}$  and Eq. (2) takes the form,

$$\beta = \frac{\ell(\ell-1) + (\ell+1)(\ell+2)(\sigma_{\ell+1}/\sigma_{\ell-1}) - 6\ell(\ell+1)(\sigma_{\ell+1}/\sigma_{\ell-1})^{1/2} \cos \phi}{(2\ell+1)[\ell + (\ell+1)(\sigma_{\ell+1}/\sigma_{\ell-1})]}, \quad (5)$$

where the linear momentum and hence eKE are accounted for in the calculation of the cross sections. This approach is tested in Fig. 2(a) for  $\mu=0$ , when Eq. (5) should become identical to Eq. (2). The series of crosses representing Eq. (5) fall exactly on the solid line generated by Eq. (2) using the same relative phase angle.

Equation (5) can now be used to account for the electron-dipole interactions. The dotted, dashed and dash-dotted lines in Fig. 2(b) were generated using Eq. (5) for the detachment of  $\text{I}^- \cdot \text{H}_2\text{O}$ ,  $\text{I}^- \cdot \text{CH}_3\text{I}$ , and  $\text{I}^- \cdot \text{CH}_3\text{CN}$ , respectively. The  $s$  and  $d$  wave cross sections were calculated using the O'Malley approach described above.<sup>74</sup> Based on the  $\text{I}\cdot\text{H}_2\text{O}$ ,  $\text{I}\cdot\text{CH}_3\text{I}$ , and  $\text{I}\cdot\text{CH}_3\text{CN}$  dipole moment values (see above),  $s$  wave emission occurs in the large- $\mu$  regime, described by Eq. (4), while for  $d$  waves the small- $\mu$  description [Eq. (3)] is appropriate. Varying  $\delta$  in Eq. (4) was found to have only a very minor effect on the  $\beta$  values and hence  $\delta$  was arbitrarily set to zero.

In the end, the experimental  $\beta$  values for  $\text{I}^- \cdot \text{CH}_3\text{I}$  still fall nowhere near the corresponding calculated curve. The disagreement persists even if the model parameters are varied within reasonable margins. Thus, it appears unlikely that the anomalously isotropic PAD in the  $\text{I}^- \cdot \text{CH}_3\text{I}$  case can be due to the electron-dipole interactions.

In summary, the adaptation<sup>69</sup> of the Cooper-Zare central-potential model<sup>51,52</sup> by Hanstorp *et al.* yields good agreement with experiment for the species studied, with the notable exception of  $\text{I}^- \cdot \text{CH}_3\text{I}$ . Admittedly, this model neglects long-range electron-dipole interactions and hence its application to the cluster species with polar solvents should be taken with caution. However, significant electron-dipole interactions are expected in the detachment of  $\text{I}^- \cdot \text{H}_2\text{O}$ ,  $\text{I}^- \cdot \text{CH}_3\text{I}$ , and  $\text{I}^- \cdot \text{CH}_3\text{CN}$ , yet only one of them,  $\text{I}^- \cdot \text{CH}_3\text{I}$ , shows an anomalous PAD. We conclude that the dipole considerations alone cannot account for the observed effect and hence the very nature of electron detachment in  $\text{I}^- \cdot \text{CH}_3\text{I}$  is likely to be different compared to the other species.

### C. Nature of $\text{I}^- \cdot \text{CH}_3\text{I}$ detachment

Most features of the reported cluster-anion photoelectron images allow a straightforward interpretation that the detachment takes place from atomic iodide solvated by a neutral atom or molecule. However,  $\text{I}^- \cdot \text{CH}_3\text{I}$  yields a surprising result, which contrasts it to all other cluster anions studied. The PAD in the  $\text{I}^- \cdot \text{CH}_3\text{I}$  case is much more isotropic than expected from simple arguments, either treating the  $\text{CH}_3\text{I}$  molecule purely as a spectator or taking the dipole moment of the neutral cluster into account. In addition, in higher-resolution energy-domain work,<sup>39</sup> the  ${}^2P_{3/2}$  transition in  $\text{I}^- \cdot \text{CH}_3\text{I}$  photodetachment seems to be uncharacteristically narrow.

In considering the anomalous lack of photodetachment anisotropy in the  $\text{I}^- \cdot \text{CH}_3\text{I}$  case, one may look for clues in the photochemical properties of the solvent molecule. An important difference in this regard between  $\text{H}_2\text{O}$  and  $\text{CH}_3\text{CN}$ , on the one hand side, and  $\text{CH}_3\text{I}$ , on the other, is that neither water nor acetonitrile absorb 267 nm light,<sup>75,76</sup> while methyl iodide does.<sup>77</sup> Regardless of the exact mechanism, the availability of accessible excited electronic states in  $\text{CH}_3\text{I}$  must be key to interpreting the experimental results.

The  $\text{I}^- \cdot \text{CH}_3\text{I}$  anion has been studied quite extensively.<sup>30,32,37-40,73,78</sup> The overall behavior of the photoabsorption cross section reflects competition between photofragmentation and photodetachment. Near the detachment threshold the  $\text{I}^- \cdot \text{CH}_3\text{I}$  photoexcitation spectrum (measured by detecting  $\text{I}^-$  fragments) displays two narrow bands separated by the spin-orbit splitting of iodine.<sup>40</sup> These correspond to electron transfer and subsequent dissociation of the  $\text{CH}_3\text{I}$  molecule. The yield of  $\text{I}^-$  photofragments from  $\text{I}^- \cdot \text{CH}_3\text{I}$  decreases rapidly above the detachment threshold, with no ionic products seen at the wavelength of the present experiment.<sup>40</sup>

On the other hand, the 267 nm photon energy is well above the dissociation limit for  $\text{CH}_3\text{I}$  (2.4 eV) and therefore one may question whether direct absorption by the solvent

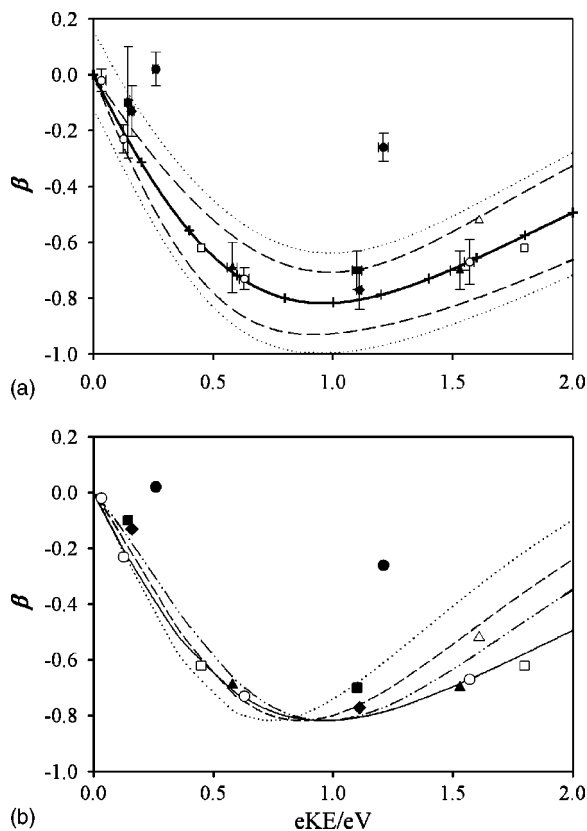


FIG. 2. Variation in anisotropy parameter  $\beta$  as a function of  $eKE$ . In (a) and (b) symbols represent experimental data, while lines show the results of theoretical modeling. Open symbols are data points for photodetachment from unsolvated  $I^-$ , while solid symbols represent monosolvated species. The same experimental data are shown in both (a) and (b), but the error bars are indicated in (a) only. Experimental data from the current study are shown as (open) circles for  $I^-$ , triangles for  $I^- \cdot Ar$ , diamonds for  $I^- \cdot H_2O$ , squares for  $I^- \cdot CH_3CN$ , and (filled) circles for  $I^- \cdot CH_3I$ . Data for  $I^-$  obtained by our group at wavelengths other than 267 nm are also included (as open circles). Additional data points for  $I^-$  from the groups of Lineberger (Ref. 71) and Neumark (Ref. 21) are shown as open squares and triangles, respectively. The solid line in (a) represents a nonlinear regression fit of Eq. (2) to the experimental data points for  $I^-$ . The crosses (+), which fall exactly on the solid curve, represent  $\beta$  values calculated using the modified approach of Eq. (5) with zero dipole moment. Also shown are the 95% confidence limits (dashed lines) and 95% prediction limits (dotted lines), determined as described in the text. The graph in (b) shows the effect of including the dipole moment of the neutral residue on the detachment anisotropy, as modeled using Eq. (5). The dotted line corresponds to  $I^- \cdot H_2O$ , dash-dotted to  $I^- \cdot CH_3I$ , and dashed to  $I^- \cdot CH_3CN$ . The  $I^-$  curve (zero dipole moment) is reproduced for reference as a solid line.

molecule followed by its dissociation plays a role in the observed dynamics. In isolated  $CH_3I$  dissociation, both  $I(^2P_{3/2})$  and  $I(^2P_{1/2})$  are produced at 266 nm, with a  $^2P_{1/2}:^2P_{3/2}$  branching ratio of 70:30.<sup>79,80</sup> In  $I^- \cdot CH_3I$ , the dissociation of the methyl iodide group would produce a methyl radical recoiling in the direction of the  $I^-$  with roughly 1–2 eV of kinetic energy depending on the final state of the iodine fragment. The  $CH_3 + I^-$  collision would occur on a repulsive potential energy surface, which crosses the neutral  $CH_3I$  potential.<sup>81</sup> The neutral surface has a minimum located 0.6 eV above the  $CH_3 + I^-$  asymptote. Thus, the energy release from the solvent dissociation is sufficient to reach the autodetachment continuum in the transient  $[CH_3I]^-$  collision complex. Subsequent autodetachment would yield a more

isotropic PAD, compared to a direct photodetachment process, consistent with the experiment. Energetically, the detachment would still occur from the same electronic state as the direct process, resulting in a photoelectron energy spectrum with the two  $I(^2P_{1/2,3/2})$  product channels. Nonetheless, while this reactive mechanism is qualitatively consistent with the overall features of the  $I^- \cdot CH_3I$  photoelectron image, it can be effectively ruled out, because the cross section for  $CH_3I$  photodissociation at 267 nm is 30–40 times smaller than that for direct photodetachment of  $I^-$ .<sup>27,82</sup>

A more plausible explanation for the anomalous PAD in the  $I^- \cdot CH_3I$  case is the existence of a scattering resonance. Experimental studies of electron-methyl iodide scattering have been carried out over a wide range of  $eKE$  (0–100 eV).<sup>83–95</sup> A resonance observed to peak at  $\sim 2$  eV in electron scattering from methyl halides has been attributed to electron capture into the  $C-X \sigma^*$  lowest unoccupied molecular orbital.<sup>83,84,93,96,97</sup> This resonance is of interest for the current data, because it falls very close to the  $^2P_{3/2}$  channel. In addition, the scattering cross section increases as the energy decreases below 0.5 eV, into the  $^2P_{1/2}$  channel domain. Thus, it does not seem unreasonable that the detached electron could be scattered from the neutral solvent molecule.

The presence of a scattering resonance is expected to affect the relative phase angle in Eq. (5), causing a change in the  $\beta$  value. Prediction using any value of  $\cos \phi$  that is independent of  $eKE$  is inadequate in this case. Benitez *et al.*<sup>93</sup> used correlation between electron transmission spectra and inner-shell excitation spectra to deduce the presence of a shape resonance in  $CH_3I$  slightly below 1 eV. Bound and continuum multiple scattering  $X\alpha$  calculations predict a low-energy resonance  $\sigma^*$  state in  $CH_3I^-$  at 1.44 and 1.22 eV, respectively. These resonances were not observed experimentally, but lie in the correct energy range to be possible explanations for the current results. Further experiments at different detachment wavelengths will be useful in ongoing study of this problem.

The behavior of the  $e^- + CH_3I$  scattering cross section at low energies is characteristic of polar molecules.<sup>83</sup> Therefore, if scattering is responsible for the anomalous lack of anisotropy in  $I^- \cdot CH_3I$  photodetachment, it is valid to question why the  $I^- \cdot H_2O$  and  $I^- \cdot CH_3CN$  images do not show similar effects. Electron scattering measurements on  $H_2O$  via a linear transmission method in the 0.5–10 eV range<sup>98</sup> show that the cross section is several times smaller than that for  $CH_3I$ . This can be seen as a reflection of the solvent molecule size. Electron scattering experiments on  $H_2O$  have failed to find evidence for resonance between 0 and 6 eV;<sup>99</sup> the lowest reported resonance, corresponding to the  $^2A_1$  state of  $H_2O^-$ , lies at  $\sim 7.9$  eV.<sup>100</sup> Electron scattering experiments on  $CH_3CN$  reveal a  $\pi^*$  shape resonance at 2.9 eV,<sup>101</sup> again significantly higher in energy than the  $eKE$ s in the present work.<sup>94</sup> Therefore, of all cluster anions studied here, electron-solvent scattering resonances can play a role only in  $I^- \cdot CH_3I$ , possibly contributing to the anomalously isotropic PAD observed in this case.

## V. SUMMARY

Photodetachment from a series of monosolvated iodide cluster anions has been studied through photoelectron imaging with particular emphasis on the spin-orbit channel branching ratios and photoelectron angular distributions. The solvated anion photoelectron images are examined in comparison to bare  $I^-$ . In the case of  $I^- \cdot Ar$ , the solvent atom has little effect on the angular distribution and the  $^2P_{1/2}$  to  $^2P_{3/2}$  channel branching ratio. In  $I^- \cdot H_2O$  photodetachment, the effect of the solvent on the PAD is consistent with the predictions of the Cooper-Zare central-potential model, once the hydration-induced energetic shift of the detachment bands is taken into account. However, the  $^2P_{1/2} : ^2P_{3/2}$  channel branching ratio is significantly affected by the presence of the polar water molecule and the excited spin-orbit channel is enhanced by more than 60% relative to the bare  $I^-$  case. This enhancement is consistent with previous cross-section measurements in hydrated iodide systems<sup>34</sup> and attributed to dipolar effects on the final-state continuum wave function. In the case of  $I^- \cdot CH_3CN$ , the  $^2P_{1/2}$  to  $^2P_{3/2}$  branching ratio is surprisingly much smaller than that for  $I^- \cdot H_2O$ , and even reduced slightly compared to bare  $I^-$ . The suppression of the  $^2P_{1/2}$  channel in  $I^- \cdot CH_3CN$  is attributed to the proximity of the  $^2P_{1/2}$  channel threshold to the photon energy used in the experiment. Also not ruled out completely is the possibility of the dipole-bound anion state of acetonitrile acting as a sink for the lowest-energy electrons.

More intriguing results are obtained for the photodetachment of  $I^- \cdot CH_3I$ . The channel branching ratio is similar to that for  $I^- \cdot H_2O$ , consistent with the model where the final-state dipole moment affects the detachment cross sections. However, the nearly isotropic PADs characteristic of both detachment channels in  $I^- \cdot CH_3I$  do not fit into the picture of direct photodetachment from the  $I^-$  cluster core, even when the dipole effects are taken into account. The alternative scenarios include a photoinduced bimolecular reaction within the cluster yielding an autodetaching product and photoelectron scattering by the solvent molecule. While the former mechanism is effectively ruled out by consideration of the small dissociation cross section (relative to detachment), electron scattering from the solvent is indeed likely to play a role, because of the existence of low lying scattering resonances in the  $CH_3I^-$  continuum.

## ACKNOWLEDGMENTS

The authors would like to acknowledge discussions with Professor Mark A. Johnson, Professor Laurie J. Butler, and Dr. Katharine L. Reid. In addition, the authors thank Professor Johnson for sending them unpublished data on  $I^- \cdot CH_3CN$  photoabsorption cross sections. This work was generously supported by the NSF Grant No. CHE-0134631, the Beckman Young Investigator Award (The Arnold and Mabel Beckman Foundation), and the Packard fellowship for Science and Engineering (The David and Lucile Packard Foundation).

- <sup>1</sup>D. W. Chandler and P. L. Houston, *J. Chem. Phys.* **87**, 1445 (1987).
- <sup>2</sup>A. J. R. Heck and D. W. Chandler, *Annu. Rev. Phys. Chem.* **46**, 335 (1995).
- <sup>3</sup>P. L. Houston, *Acc. Chem. Res.* **28**, 453 (1995).
- <sup>4</sup>K. M. Ervin and W. C. Lineberger, in *Advances in Gas Phase Ion Chemistry*, edited by N. G. Adams and L. M. Babcock (JAI, Greenwich, 1992), Vol. 1, p. 121.
- <sup>5</sup>B. Baguenard, J. C. Pinare, C. Bordas, and M. Broyer, *Phys. Rev. A* **63**, 023204 (2001).
- <sup>6</sup>E. Surber and A. Sanov, *Phys. Rev. Lett.* **90**, 093001 (2003).
- <sup>7</sup>D. M. Neumark (private communication).
- <sup>8</sup>E. Surber and A. Sanov, *J. Chem. Phys.* **116**, 5921 (2002).
- <sup>9</sup>E. Surber, R. Mabbs, and A. Sanov, *J. Phys. Chem. A* **107**, 8215 (2003).
- <sup>10</sup>R. Mabbs, E. Surber, and A. Sanov, *Chem. Phys. Lett.* **381**, 479 (2003).
- <sup>11</sup>B. Baguenard, J. C. Pinare, F. Lepine, C. Bordas, and M. Broyer, *Chem. Phys. Lett.* **352**, 147 (2002).
- <sup>12</sup>A. K. Luong, T. G. Clements, M. S. Resat, and R. E. Continetti, *J. Chem. Phys.* **114**, 3449 (2001).
- <sup>13</sup>H. J. Deyerl, L. S. Alconcel, and R. E. Continetti, *J. Phys. Chem. A* **105**, 552 (2001).
- <sup>14</sup>E. Surber and A. Sanov, *J. Chem. Phys.* **118**, 9192 (2003).
- <sup>15</sup>E. Surber, S. P. Ananthavel, and A. Sanov, *J. Chem. Phys.* **116**, 1920 (2002).
- <sup>16</sup>E. Surber, R. Mabbs, T. Habteyes, and A. Sanov (unpublished).
- <sup>17</sup>R. Mabbs, E. Surber, and A. Sanov, *Analyst (Cambridge, U.K.)* **128**, 765 (2003).
- <sup>18</sup>R. Mabbs, E. Surber, L. Velarde, and A. Sanov, *J. Chem. Phys.* **120**, 5148 (2004).
- <sup>19</sup>B. J. Greenblatt, M. T. Zanni, and D. M. Neumark, *Science* **276**, 1675 (1997).
- <sup>20</sup>A. Stolow, A. E. Bragg, and D. M. Neumark, *Chem. Rev. (Washington, D.C.)* **104**, 1719 (2004).
- <sup>21</sup>A. V. Davis, R. Wester, A. E. Bragg, and D. M. Neumark, *J. Chem. Phys.* **118**, 999 (2003).
- <sup>22</sup>R. Mabbs, K. Pichugin, E. Surber, and A. Sanov, *J. Chem. Phys.* **121**, 265 (2004).
- <sup>23</sup>A. W. Castleman and K. H. Bowen, *J. Phys. Chem.* **100**, 12911 (1996).
- <sup>24</sup>A. Sanov and W. C. Lineberger, *PhysChemComm* **5**, 165 (2002).
- <sup>25</sup>A. Sanov and W. C. Lineberger, *Phys. Chem. Chem. Phys.* **6**, 2018 (2004).
- <sup>26</sup>C. E. Moore, *Atomic Energy Levels* (National Bureau of Standards, Washington, DC, 1958).
- <sup>27</sup>A. Mandl and H. A. Hyman, *Phys. Rev. Lett.* **31**, 417 (1973).
- <sup>28</sup>E. J. Robinson and S. Geltman, *Phys. Rev.* **153**, 4 (1967).
- <sup>29</sup>M. A. Johnson (private communication).
- <sup>30</sup>C. E. H. Dessent, C. G. Bailey, and M. A. Johnson, *J. Chem. Phys.* **103**, 2006 (1995).
- <sup>31</sup>C. G. Bailey, C. E. H. Dessent, M. A. Johnson, and K. H. Bowen, *J. Chem. Phys.* **104**, 6976 (1996).
- <sup>32</sup>D. M. Cyr, M. G. Scarton, and M. A. Johnson, *J. Chem. Phys.* **99**, 4869 (1993).
- <sup>33</sup>Y. X. Zhao, I. Yourshaw, G. Reiser, C. C. Arnold, and D. M. Neumark, *J. Chem. Phys.* **101**, 6538 (1994).
- <sup>34</sup>D. Serxner, C. E. H. Dessent, and M. A. Johnson, *J. Chem. Phys.* **105**, 7231 (1996).
- <sup>35</sup>C. Bassmann, U. Boesl, D. Yang, G. Drechsler, and E. W. Schlag, *Int. J. Mass Spectrom. Ion Processes* **159**, 153 (1996).
- <sup>36</sup>M. Kowal, R. W. Gora, S. Roszak, and J. Leszczynski, *J. Chem. Phys.* **115**, 9260 (2001).
- <sup>37</sup>D. M. Cyr, G. A. Bishea, M. G. Scarton, and M. A. Johnson, *J. Chem. Phys.* **97**, 5911 (1992).
- <sup>38</sup>D. M. Cyr, C. G. Bailey, D. Serxner, M. G. Scarton, and M. A. Johnson, *J. Chem. Phys.* **101**, 10507 (1994).
- <sup>39</sup>C. C. Arnold, D. M. Neumark, D. M. Cyr, and M. A. Johnson, *J. Phys. Chem.* **99**, 1633 (1995).
- <sup>40</sup>C. E. H. Dessent, C. G. Bailey, and M. A. Johnson, *J. Chem. Phys.* **105**, 10416 (1996).
- <sup>41</sup>G. Markovich, L. Perera, M. L. Berkowitz, and O. Cheshnovsky, *J. Chem. Phys.* **105**, 2675 (1996).
- <sup>42</sup>C. E. H. Dessent, J. Kim, and M. A. Johnson, *Acc. Chem. Res.* **31**, 527 (1998).
- <sup>43</sup>Q. K. Timerghazin and G. Pelsherbe, *Chem. Phys. Lett.* **354**, 31 (2002).
- <sup>44</sup>M. A. Johnson and W. C. Lineberger, in *Techniques for the Study of Ion*

- Molecule Reactions*, edited by J. M. Farrar and W. H. Saunders (Wiley, New York, 1988), p. 591.
- <sup>45</sup>M. E. Nadal, P. D. Kleiber, and W. C. Lineberger, *J. Chem. Phys.* **105**, 504 (1996).
- <sup>46</sup>A. T. J. B. Eppink and D. H. Parker, *Rev. Sci. Instrum.* **68**, 3477 (1997).
- <sup>47</sup>W. C. Wiley and I. H. McLaren, *Rev. Sci. Instrum.* **26**, 1150 (1955).
- <sup>48</sup>V. Dribinski, A. Ossadtchi, V. A. Mandelshtam, and H. Reisler, *Rev. Sci. Instrum.* **73**, 2634 (2002).
- <sup>49</sup>A. D. Dickson, I. M. Mills, and B. Crawford, Jr., *J. Chem. Phys.* **27**, 445 (1957).
- <sup>50</sup>J. Cooper and R. N. Zare, in *Atomic Collision Processes*, edited by S. Geltman, K. T. Mahanthappa, and W. E. Brittin (Gordon and Breach, New York, 1968), Vol. XI-C, p. 317.
- <sup>51</sup>J. Cooper and R. N. Zare, *J. Chem. Phys.* **48**, 942 (1968).
- <sup>52</sup>J. Cooper and R. N. Zare, *J. Chem. Phys.* **49**, 4252 (1968).
- <sup>53</sup>*CRC Handbook of Chemistry and Physics*, 84th ed. (CRC, Boca Raton, FL, 2004).
- <sup>54</sup>E. P. Wigner, *Phys. Rev.* **73**, 1002 (1948).
- <sup>55</sup>J. W. Farley, *Phys. Rev. A* **40**, 6286 (1989).
- <sup>56</sup>S. Geltman, *Phys. Rev.* **104**, 346 (1956).
- <sup>57</sup>M. M. Klien and K. A. Bruekner, *Phys. Rev.* **111**, 1115 (1958).
- <sup>58</sup>J. W. Cooper and J. B. Martin, *Phys. Rev.* **126**, 1482 (1962).
- <sup>59</sup>B. H. Armstrong, *Phys. Rev.* **131**, 1132 (1963).
- <sup>60</sup>S. A. Adelman, *Phys. Rev. A* **5**, 508 (1972).
- <sup>61</sup>T. L. John and A. R. Williams, *J. Phys. B* **5**, 1662 (1972).
- <sup>62</sup>K. J. Reed, A. H. Zimmerman, H. C. Andersen, and J. I. Brauman, *J. Chem. Phys.* **64**, 1368 (1976).
- <sup>63</sup>R. M. Stehman and S. B. Woo, *Phys. Rev. A* **20**, 281 (1979).
- <sup>64</sup>V. K. Ivanov, *J. Phys. B* **32**, R67 (1999).
- <sup>65</sup>W. R. Johnson and C. D. Lin, *Phys. Rev. A* **20**, 964 (1979).
- <sup>66</sup>V. Radojevic, H. P. Kelly, and W. R. Johnson, *Phys. Rev. A* **35**, 2117 (1987).
- <sup>67</sup>M. Kutzner, J. T. Brown, and J. Thorarinson, *Phys. Rev. A* **68**, 042713 (2003).
- <sup>68</sup>W. Sailer, A. Pelc, P. Lima-Viera, N. J. Mason, J. Limtrakul, P. Scheier, M. Probst, and T. D. Mark, *Chem. Phys. Lett.* **381**, 216 (2003).
- <sup>69</sup>D. Hanstorp, C. Bengtsson, and D. J. Larson, *Phys. Rev. A* **40**, 670 (1989).
- <sup>70</sup>P. R. Gill, W. Murray, and M. H. Wright, in *Practical Optimization* (Academic, London, 1981), p. 136.
- <sup>71</sup>M. K. Gilles, K. M. Ervin, J. Ho, and W. C. Lineberger, *J. Phys. Chem.* **96**, 1130 (1992).
- <sup>72</sup>M. J. Frisch, G. W. Trucks, H. B. Schlegel *et al.*, GAUSSIAN 98, Gaussian, Inc., Pittsburgh, PA, 1998.
- <sup>73</sup>W.-P. Hu and D. G. Truhlar, *J. Phys. Chem.* **98**, 1049 (1994).
- <sup>74</sup>T. F. O'Malley, *Phys. Rev.* **137**, A1668 (1965).
- <sup>75</sup>M. N. R. Ashfold, M. T. Macpherson, and J. P. Simons, in *Topics in Current Chemistry* (Springer, Berlin, 1979), Vol. 86, p. 1.
- <sup>76</sup>M. Moriyama, Y. Tsutsui, and K. Honma, *J. Chem. Phys.* **108**, 6215 (1998).
- <sup>77</sup>R. S. Mulliken, *Phys. Rev.* **47**, 413 (1935).
- <sup>78</sup>R. Wester, A. E. Bragg, A. V. Davis, and D. M. Neumark, *J. Chem. Phys.* **119**, 10032 (2003).
- <sup>79</sup>K. Q. Lao, M. D. Person, P. Xayariboun, and L. J. Butler, *J. Chem. Phys.* **92**, 823 (1990).
- <sup>80</sup>W. P. Hess, S. J. Kohler, H. K. Haugen, and S. R. Leone, *J. Chem. Phys.* **84**, 2143 (1986).
- <sup>81</sup>J. Kim, J. A. Kelley, P. Ayotte, S. B. Nielsen, G. H. Weddle, and M. A. Johnson, *J. Am. Soc. Mass Spectrom.* **10**, 810 (1999).
- <sup>82</sup>M. Dzvonik, S. Yang, and R. Bersohn, *J. Chem. Phys.* **61**, 4408 (1974).
- <sup>83</sup>M. Kimura, O. Sueoka, C. Makochekanwa, H. Kawate, and M. Kawada, *J. Chem. Phys.* **115**, 7442 (2001).
- <sup>84</sup>C. Szmytkowski and A. M. Krzysztofowicz, *Chem. Phys. Lett.* **209**, 474 (1993).
- <sup>85</sup>M. Volkmer, C. Meier, A. Mihill, M. Fink, and N. Bowering, *Phys. Rev. Lett.* **68**, 2289 (1992).
- <sup>86</sup>D. Spence and G. J. Schulz, *J. Chem. Phys.* **58**, 1800 (1973).
- <sup>87</sup>J. A. Stockdale, F. J. Davis, R. N. Compton, and C. E. Klots, *Chem. Phys.* **60**, 4279 (1974).
- <sup>88</sup>E. Algle, N. G. Adams, and D. Smith, *J. Phys. B* **17**, 3827 (1984).
- <sup>89</sup>H. Shimamori and Y. Nakatani, *Chem. Phys. Lett.* **150**, 109 (1988).
- <sup>90</sup>H. Shimamori, Y. Tatsumi, Y. Ogawa, and T. Sumagawa, *Chem. Phys. Lett.* **194**, 223 (1992).
- <sup>91</sup>S. H. Alajajian, M. T. Bernius, and A. Chutjian, *J. Phys. B* **21**, 4021 (1988).
- <sup>92</sup>D. Spence, *J. Chem. Phys.* **66**, 669 (1977).
- <sup>93</sup>A. Benitez, J. H. Moore, and J. A. Tossell, *J. Chem. Phys.* **88**, 6691 (1988).
- <sup>94</sup>A. Modelli, F. Scagnolari, G. Distefano, D. Jones, and M. Guerra, *J. Chem. Phys.* **96**, 2061 (1992).
- <sup>95</sup>I. V. Sushanin, S. M. Kishko, and P. V. Feltsan, *Opt. Spectrosc.* **66**, 275 (1989).
- <sup>96</sup>P. D. Burrow, A. Modelli, N. S. Chiu, and K. D. Jordan, *J. Chem. Phys.* **77**, 2699 (1982).
- <sup>97</sup>M. Guerra, D. Jones, G. Distefano, F. Scagnolari, and A. Modelli, *J. Chem. Phys.* **94**, 484 (1991).
- <sup>98</sup>C. Szmytkowski, *Chem. Phys. Lett.* **136**, 363 (1987).
- <sup>99</sup>L. Sanche and G. J. Schulz, *J. Chem. Phys.* **58**, 479 (1973).
- <sup>100</sup>D. Mathur and J. B. Hasted, *Chem. Phys. Lett.* **34**, 90 (1975).
- <sup>101</sup>P. D. Burrow, A. E. Howard, A. R. Johnston, and K. D. Jordan, *J. Phys. Chem.* **96**, 7570 (1992).